International Journal of Pharmaceutics 653 (2024) 123882

Contents lists available at ScienceDirect

International Journal of Pharmaceutics

journal homepage: www.elsevier.com/locate/ijpharm

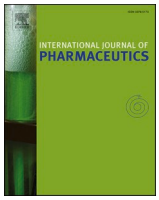

Conjugation to gold nanoparticles of methionine gamma-lyase, a cancer-starving enzyme. Physicochemical characterization of the nanocomplex for prospective nanomedicine applications

Samanta Raboni [a,b,*,1], Francesco Fumagalli [c,1], Giacomo Ceccone [c], Rita La Spina [c], Jessica Ponti [c], Dora Mehn [c], Giuditta Guerrini [c], Stefano Bettati [b,d,e], Andrea Mozzarelli [b], Mario D'Acunto [b], Gianluca Presciuttini [b], Caterina Cristallini [f], Edi Gabellieri [b], Patrizia Cioni [b]

[a] Department of Food and Drug, University of Parma, Parco Area delle Scienze 23/A, 43124 Parma, Italy
[b] Institute of Biophysics, IBF Pisa – CNR, via G. Moruzzi, 1, 56124 Pisa, Italy
[c] European Commission, Joint Research Centre (JRC), Via Enrico Fermi, 2749, 21027 Ispra, Italy
[d] Department of Medicine and Surgery, University of Parma, Via Volturno 39, 43126 Parma, Italy
[e] Interdepartmental Center Biopharmanet-TEC, University of Parma, Parma, Italy
[f] Institute for Chemical and Physical Processes, IPCF Pisa – CNR, Largo Lucio Lazzarino 2, 56122 Pisa, Italy

ARTICLE INFO

Keywords:
Gold nanoparticles
Protein nanoparticle interactions
Enzyme-based cancer therapeutics
Methionine depletion
Immobilized enzyme

ABSTRACT

The pyridoxal 5′-dependent enzyme methionine γ-lyase (MGL) catalyzes the degradation of methionine. This activity has been profitable to develop an antitumor agent exploiting the strict dependence of most malignant cells on the availability of methionine. Indeed, methionine depletion blocks tumor proliferation and leads to an increased susceptibility to anticancer drugs. Here, we explore the conjugation of MGL to gold nanoparticles capped with citrate (AuNPs) as a novel strategy to deliver MGL to cancer cells. Measurements of Transmission Electron Microscopy, Dynamic Light Scattering, Asymmetrical Flow Field-Flow Fractionation, X-ray Photoelectron Spectroscopy, and Circular Dichroism allowed to achieve an extensive biophysical and biochemical characterization of the MGL-AuNP complex including particle size, size distribution, MGL loading yield, enzymatic activity, and impact of gold surface on protein structure. Noticeably, we found that activity retention was improved over time for the enzyme adsorbed to AuNPs with respect to the enzyme free in solution. The acquired body of knowledge on the nanocomplex properties and this encouraging stabilizing effect upon conjugation are the necessary basis for further studies aimed at the evaluation of the therapeutic potential of MGL-AuNP complex in a biological milieu.

1. Introduction

In quest for innovative and selective anticancer strategies, the use of enzymes causing starvation-induced cancer cell death through removal of essential nutrients is gaining recognition (Cioni et al., 2022; Fernandes et al., 2017; Fung and Chan, 2017). Indeed, the FDA-approved therapeutic administration of asparaginase, an asparagine-degrading enzyme, for the treatment of acute lymphocytic leukemia is based on cancer cells strong dependence on asparagine, and firstly acknowledged the power and applicability of such nutrient deprivation strategy (Cioni et al., 2022). In this context, the pyridoxal 5′-phosphate (PLP)-dependent enzyme methionine γ-lyase (EC 4.4.1.11, MGL), which degrades L-methionine to α-ketobutyrate, methanethiol and ammonia via γ-elimination, can be envisaged as a potential antineoplastic agent (Cavuoto and Fenech, 2012), since the proliferation of most malignant cells, differently from normal cells, is strongly dependent on exogenous methionine supply (Chaturvedi et al., 2018; Hoffman and Erbe, 1976). The *in vitro* and *in vivo* efficiency and efficacy of MGL against various

* Corresponding author at: Department of Food and Drug, University of Parma, Parco Area delle Scienze 23/A, 43124 Parma, Italy.
E-mail addresses: samanta.raboni@unipr.it (S. Raboni), francesco-sirio.fumagalli@ec.europa.eu (F. Fumagalli), giacomo.ceccone@ec.europa.eu (G. Ceccone), rita.la-spina@ec.europa.eu (R. La Spina), jessica.ponti@ec.europa.eu (J. Ponti), dora.mehn@ec.europa.eu (D. Mehn), giuditta.guerrini@ec.europa.eu (G. Guerrini), stefano.bettati@unipr.it (S. Bettati), andrea.mozzarelli@unipr.it (A. Mozzarelli), mario.dacunto@ibf.cnr.it (M. D'Acunto), gianluca.presciuttini@ibf.cnr.it (G. Presciuttini), caterina.cristallini@cnr.it (C. Cristallini), edi.gabellieri@ibf.cnr.it (E. Gabellieri), patrizia.cioni@ibf.cnr.it (P. Cioni).
[1] Contributed equally to this work.

https://doi.org/10.1016/j.ijpharm.2024.123882
Received 18 July 2023; Received in revised form 2 February 2024; Accepted 3 February 2024
Available online 10 February 2024

cancer types has been widely demonstrated (El-Sayed, 2010; Hoffman, 2015, 2019; Tan et al., 2010) and lately reviewed (Cioni et al., 2022; Raboni et al., 2024). It is well proven that MGL in solution specifically affects cultured cancer cell proliferation and survival, while it does not significantly perturb non-malignant cells (Kulikova et al., 2017; Morozova et al., 2013; Raboni et al., 2018). Insights into cellular and molecular events occurring during MGL-mediated methionine starvation of cancer cells have been recently provided by histone modifications and proteomic profiling studies (Montalbano et al., 2023; Raboni et al., 2021). Besides, inclusion of MGL in different nanoporous or vesicular systems (Gay et al., 2017; Koval et al., 2022; Machover et al., 2019; Morozova et al., 2018; Xin et al., 2021) has been tested *in vitro* to assess the effects on its functional and structural properties, and on cultured cancer cells and/or in mouse models for therapeutic efficacy. Indeed, immobilization to solid matrices may help to overcome the multiple challenges (Dean et al., 2017) that the development of enzyme-based therapeutics needs to face (de la Fuente et al., 2021; Marchetti et al., 2022).

In this context, the possibility of applying the emerging knowledge and tools of nanotechnology to pharmaceutical and biomedical sciences is an attracting opportunity for the development of nanocomplexes loaded with proteins/enzymes (but also small-molecule drugs and imaging agents) endowed with high efficacy and safety (Anselmo and Mitragotri, 2016; Kopp et al., 2017; Shi et al., 2017; Tong and Kohane, 2016) for drug delivery and as diagnostics (Mitchell et al., 2021).

In this regard, gold nanoparticles have become more and more attractive for multiple applications in biomedical research (Ajnai et al., 2014; D'Acunto et al., 2021; Jazayeri et al., 2016; Yeh et al., 2012) due to biocompatibility, preferential accumulation in tumor districts, and peculiar and tunable optical properties (Sengani et al., 2017). In addition, gold nanoparticles are also enticing for their easy synthesis through the well-established protocol of reduction of auric acid by sodium citrate (Turkevich et al., 1951), a cheap, nontoxic, highly biodegradable, and biocompatible reactant, which responds to the growing need for eco-friendly synthesis processes. With its negatively charged carboxylates, citrate provides charge stabilization of the gold nanoparticles (Al-Johani et al., 2017; Park and Shumaker-Parry, 2014), but it is easily displaced/replaced by proteins due to weak interactions with the gold surface. Notably, the easily and widely functionalizable surface of the particles promotes physical or chemical conjugation with numerous biomolecules such as peptides and proteins in conditions compatible with their stability (Amina and Guo, 2020; Ielo et al., 2021). Association of proteins with gold nanoparticles may thus be useful for loading proteins as cargo, for active targeting through engagement with tumor surface receptors and eventually cellular internalization (Amina and Guo, 2020; Dreaden et al., 2011; Ghosh et al., 2010).

Interestingly, as other nanocarriers AuNPs have been reported to exert different actions in protein-dependent contexts: they may either favorably stabilize protein against denaturation (Bailes et al., 2012; Capomaccio et al., 2016; Chatterjee et al., 2021; Verma et al., 2021) and/or aggregation (Brancolini et al., 2019; Park, 2020) or cause protein denaturation and loss of function (Gagner et al., 2011; Gagner et al., 2012; Kumar and Dhawan, 2019; Tadepalli et al., 2017; Xia et al., 2020). Therefore, the biophysical and biochemical characterization of protein-coated AuNPs is of paramount importance to gather a deep understanding of the structure, composition, and function of the nanocomplex (Ceccone and Shard, 2016; Hodoroaba et al., 2020; La Spina et al., 2017).

Therefore, the present study describes for the first time, to the best of our knowledge, the functionalization of 20-nm citrate-capped gold nanoparticles (AuNPs) with prokaryotic MGL to create nanomaterials endowed with methionine depletion capability and establishes the structural and functional implications of the formation of the nanocomplex on the enzyme integrity.

The MGL-AuNP complex was investigated by UV–visible absorption, Circular Dichroism (CD) and X-ray Photoelectron Spectroscopy (XPS), Transmission Electron Microscopy (TEM), Dynamic Light Scattering (DLS), Asymmetric Flow Field Flow Fractionation (AF4), and by assaying MGL enzymatic activity. This extensive investigation enlightens successful binding of active MGL to AuNPs and MGL activity retention over time in the complex, and paves the way for the assessment of its potential in more complex and more representative biological media.

2. Results and discussion

2.1. Characterization of citrate-capped gold nanoparticles (AuNPs)

Synthesis and purification of AuNPs are described in the experimental section. Since spectrum features of the surface plasmon resonance (SPR) band such as maximum absorption wavelength (λ_{SPR}) and intensity are directly related to particle size, shape, and surface coating, UV–vis absorption measurements provide a simple and prompt method to characterize AuNPs (Ghosh and Pal, 2007; Haiss et al., 2007; Mulvaney, 1996; Shard et al., 2018). Fig. 1a shows the typical UV–vis absorption spectrum of the purified AuNPs, with the SPR band centered at 522 ± 0.5 nm. Comparison between measurements performed before and after the purification process indicates no changes in the shape and intensity of the absorption spectrum and a very small shift of λ_{SPR} (Fig. 1a, inset) assuring that the centrifugation procedure left AuNPs practically unaltered in size and shape. The diameter of purified AuNPs was estimated by measuring the ratio between the absorbance at the maximum of SPR band (A_{spr}) and the absorbance at 450 nm (A_{450}) (Haiss et al., 2007). Different AuNP preparations provide $A_{spr}/A_{450} = 1.68 \pm 0.02$, corresponding to a theoretical diameter of about 18.0 ± 0.2 nm (Haiss et al., 2007). AuNP concentration is calculated from A_{450} by using the molar extinction coefficient $3.87 \times 10^8\ M^{-1}\ cm^{-1}$, as estimated for gold nanoparticles with 18 nm diameter (Haiss et al., 2007). AuNP suspensions with concentration around 6.5×10^{-8} M were regularly obtained. The estimated AuNP size based on SPR band spectral features was confirmed by TEM (Fig. 1b-c) and DLS (Fig. 1d) experiments. TEM images automated statistics (over around 350 particles) reveals a narrow, symmetric distribution of high-contrast spherical objects that can be associated to spherical, metallic NPs with mean primary size around 18.4 nm and a FWHM of 2.4 nm. DLS measurements show an intensity based hydrodynamic diameter distribution of NPs exhibiting a slightly higher but rather similar mean and mode with a marked asymmetry in the right end tail (see Table SI1 for numerical values) resulting in a larger median size of ca. 23.7 ± 0.5 nm. The tendency for DLS intensity-based distribution to report large-size skewed distributions is well reported in literature (Souza et al., 2015; Wilson and Prud'homme, 2021) and it is not necessarily linked to the presence of aggregates but rather to the stronger scattering by larger particles. Large field of view SEM images displayed in fact AuNPs of approximately spherical shape with homogeneous size distribution and absence of aggregates (Fig. SI1). It is worth mentioning that, since these techniques measure different properties (the bare core size of the nanoparticle by electron microscopy, the hydrodynamic diameter by DLS), differences in the estimated sizes may occur (and, at certain extent, are expected).

Given that the physicochemical characterization carried out does not show a consistent presence of aggregates, purified AuNPs were used without further manipulation, such as sonication and/or addition of detergents.

2.2. Characterization of MGL binding to AuNPs

Preliminary attempts of MGL conjugation through EDC/NHS chemistry to PEGylated AuNPs showed strong perturbing effects resulting in unsatisfactory conjugation yield and strongly reduced catalytic activity for MGL (data not shown). This unfortunate, but not totally unexpected result is in line with the fact that while covalent attachment allows stable coupling of proteins to AuNPs, it may have strong consequences on the catalytic activity. This can be due to restriction of enzyme

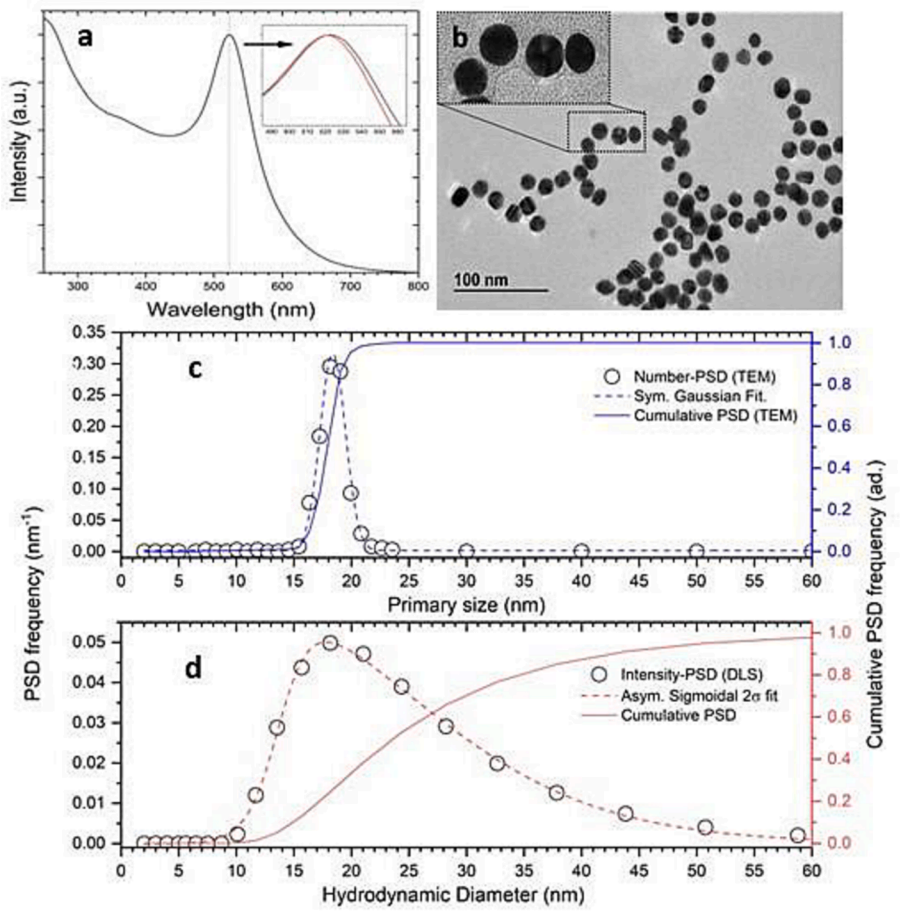

Fig. 1. Characterization of purified AuNPs. a) UV–vis spectrum of AuNPs in MilliQ water. Inset shows the spectra before (black line) and after (red line) the AuNP purification process; b) TEM images of purified AuNPs measured at 120 kV; c) purified AuNPs size frequency distribution measured via TEM (right axis, cumulative distribution); d) purified AuNPs intensity-based distribution measured via DLS images (right axis, cumulative distribution). (For interpretation of the references to color in this figure legend, the reader is referred to the web version of this article.)

conformational freedom, steric constraints and involvement of catalytic residues. On the contrary, structural and functional properties of the enzyme cargo may be less disturbed by non-covalent conjugation. Indeed, spontaneous adsorption is a more straightforward route and a facile method that only requires simple mixing of AuNPs with the protein of interest, under predetermined optimal conditions, reducing invasive manipulation steps. In our experience, physical absorption of MGL to AuNPs was more successful and was thus preferred over covalent conjugation.

At physiological pH, MGL is an anionic protein. The theoretical isoelectric point (pI), as calculated from the amino acid sequence by the ProtParam tool of ExPASy (Gasteiger, 2005) is 5.53. Above this pH, the protein has a negative net charge, which increases as pH increases. At physiological pH, AuNPs are negatively charged as the three carboxylic groups of citrate exhibit pK_a equal to 3.14, 4.77 and 6.39. As adsorption of proteins on gold nanoparticles appears to be mostly driven by electrostatic interactions (Wang et al., 2016), the binding between MGL and AuNPs is favored at pH values lower than the protein pI. Indeed, no binding of MGL to AuNPs was observed at pH 8, as verified by agarose gel electrophoresis (data not shown). However, since MGL stability decreases as pH decreases, the adsorption of MGL on AuNPs was carried out at pH 6, as a compromise, to reduce electrostatic repulsion and preserve protein structure.

Given the high sensitivity of λ_{SPR} to changes of electron distribution on the nanoparticle surface, UV–vis absorption spectroscopy is an effective technique to monitor the interaction of proteins with AuNPs and evaluate the binding affinity (Yang et al., 2013). Fig. 2a shows the absorption spectra of AuNPs in the presence of increasing amounts of MGL. No rising in the spectrum baseline is observed at increasing protein concentrations. This finding suggests that addition of MGL does not induce nanoparticle aggregation, or at least not enough to affect the light scattering signal and the spectrum shape. When MGL concentration increases, λ_{SPR} shifts gradually from 522 nm to 527 nm (Fig. 2a, inset) concomitantly with an increase up to 20 % in the absorbance intensity, as measured by integrating the area of the spectrum in the region from 450 nm to 700 nm. Both λ_{SPR} and absorbance values reach a plateau when MGL concentration is higher than 0.2×10^{-6} M, suggesting that saturation of binding sites for the protein on the AuNP surface is obtained. No significant λ_{SPR} shift or intensity increase in the surface plasmon resonance band were observed when the conjugation experiment was conducted at pH 8 (Fig. SI2), confirming the relevance of the charge on the MGL surface to determine the protein binding on AuNPs.

The Langmuir adsorption isotherm model is usually applied to analyze the interaction between proteins and AuNPs, although its application requires some caution (Latour, 2015). Firstly, the Langmuir model requires the system to be in equilibrium, that is, the adsorption of the protein onto nanoparticles is reversible during the experimental time, as it is this case, where the interaction of proteins with the AuNPs is mainly of an electrostatic type. Only over time, most of the adsorbed protein molecules irreversibly bind to AuNPs (Wang et al., 2016) presumably because of the irreversible oxidation of cysteines on the AuNP surface (Wang et al., 2014). The second warning is the use of the total

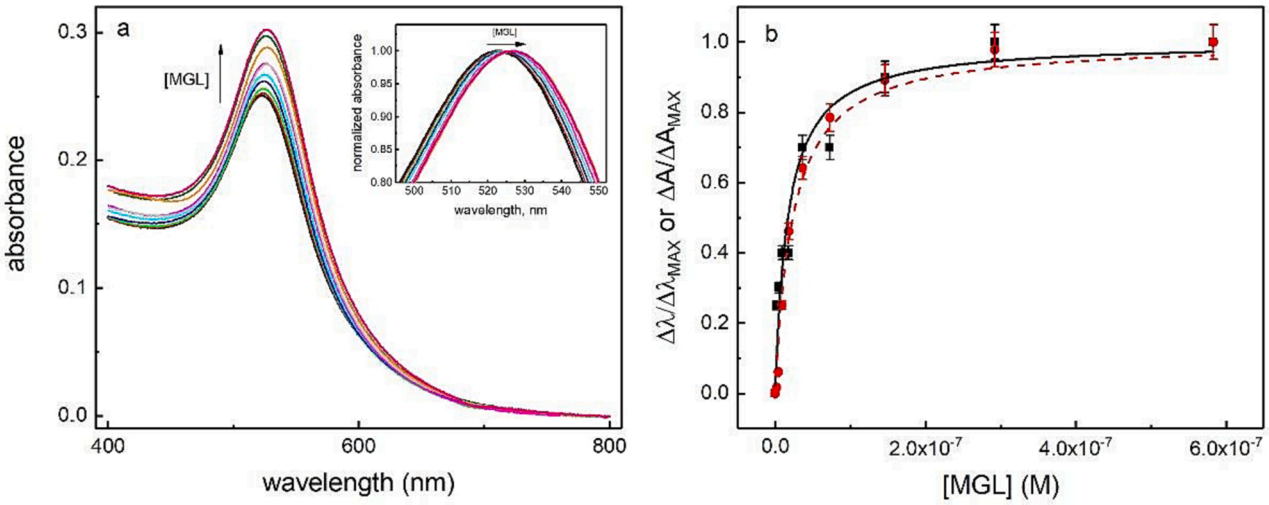

Fig. 2. Changes in AuNP absorption spectrum at increasing concentrations of MGL. a) Absorption spectra of AuNPs suspensions in the absence and presence of different concentrations of MGL. Inset shows AuNP spectral shift at increasing MGL concentration. b) Relative maximum absorption wavelength shift (squares, solid line) and absorbance increase (circles, dash line) fitted to a Langmuir adsorption isotherm model. [AuNP] = 4.5×10^{-10} M; 0 < [MGL] < 5.8×10^{-7} M; buffer is 10 mM BTM, pH 6, in the presence of 10 μM pyridoxal 5′-phosphate (PLP), the MGL cofactor. All spectra were acquired at room temperature and corrected for the PLP contribution to the absorbance.

protein concentration instead of that of the free protein, as required by the Langmuir model. This approximation is justified by the small concentration of AuNPs (0.45 nM) as compared to that of the protein (Fig. 2a). Assuming that the observed spectrum changes are entirely due to binding of MGL to AuNPs, the association constant of the interaction is estimated by fitting the λ_{SPR} shift data to a Langmuir isotherm (Yang et al., 2013).

$$\Delta\lambda/\Delta\lambda_{\max} = K_a[MGL]_{free}/\left(1 + K_a[MGL]_{free}\right) \quad (1)$$

where $\Delta\lambda$ is the shift in λ_{SPR} measured at a given MGL concentration and $\Delta\lambda_{max}$ is the maximum shift measured, in our case $\Delta\lambda_{max} = 5$ nm. K_a is the association constant whose inverse is equivalent to the protein concentration required to reach the half-maximum effect, i.e., the saturation of half of the binding sites on the AuNPs. The trend of $\Delta\lambda/\Delta\lambda_{max}$ with respect to MGL concentration is shown in Fig. 2b. Fitting the experimental data of Fig. 2b to Eq. (1) produces a K_a equal to $(5.9 \pm 1.0) \times 10^7$ M^{-1}. An independent and comparable estimate of K_a ($K_a = (4.3 \pm 0.5) \times 10^7$ M^{-1}) is obtained from the change in absorbance intensity by replacing in Eq. (1) $\Delta\lambda$ with ΔA (increase in integrated absorbance measured at a given MGL concentration), and $\Delta\lambda_{max}$ with ΔA_{max} (maximum absorbance increase measured at the plateau) (Fig. 2b). The estimated K_a is in agreement with values reported in literature for the adsorption of proteins such as bovine serum albumin (Vangala et al., 2012) or α-synuclein (Yang et al., 2013) on AuNPs of comparable hydrodynamic diameter.

2.3. Purification and biochemical characterization of MGL-AuNP complex

According to the aforementioned estimated K_a value, the MGL concentration ensures over 95 % AuNP saturation during the conjugation reaction. Removal of unbound or loosely bound MGL was obtained by centrifugation (10,000 g for 10 min), following the scheme shown in Fig. SI3. It is worth mentioning that the suspension of AuNPs precipitates rapidly even under mild centrifugation conditions in the conjugation buffer (10 mM BTM/10 μM PLP, pH 6) in the absence of MGL, and, differently from in water, it forms aggregates difficult to disperse. This finding may not be surprising because it is known that addition of electrolytes decreases the stability of metal particle suspensions as they mask the citrate negative charges causing an imbalance between repulsive and attractive forces (Derjaguin, 1941; Verwey, 1948). As a result, the colloids collapse when the gold nanoparticles adsorb onto one another to produce aggregates. However, polymeric coatings are reported to act as a physical barrier to prevent nanoparticle aggregation (Moore et al., 2015). The hydrophilic nature of several polymers such as poly(ethylene glycol) or poly(vinylpyrrolidone) imparts colloidal stabilization through short-range repulsive hydration forces (Guerrini et al., 2018). Similarly, adsorption of proteins, which contain numerous charged groups, can provide nanoparticles with steric and electrostatic stabilization. Indeed, our observation that there is no evidence of AuNPs aggregation after centrifugation in the conjugation buffer upon addition of MGL agrees with a stabilizing effect of protein on AuNPs colloid. However, to minimize possible aggregation processes, only two centrifugation steps at 10,000 g for 10 min at 20 °C were used to remove unbound MGL. Typical UV–vis absorption spectra of supernatants recovered from the first (S1) and second (S2) centrifugation step and the pellet of the second centrifugation (P2) are shown in Fig. SI4. The unaltered shape of the AuNPs spectra after the purification steps suggests the absence of nanoparticle aggregation. After each purification step, the amount of MGL and AuNPs is estimated from the absorbance measured at 280 nm and 450 nm, respectively. Due to the mild centrifugation conditions applied, the AuNPs are incompletely pelleted in each centrifugation step and only 50 % of the starting amount is collected as pellet (P2) at the end of the purification procedure. MGL activity on each fraction is measured by the discontinuous colorimetric assay with 2,4-dinitrophenylhydrazine (DNPH). As estimated by both the A_{280} and activity measurements, about 90 % of the initial amount of MGL is collected in S1 and only 3–4 % remains in S2. Interestingly, the specific activity in S1 (4.9 U mg^{-1}) and S2 (5.1 U mg^{-1}) is almost unchanged with respect to MGL in solution (5.3 U mg^{-1}), suggesting that the transient electrostatic interactions with AuNPs and/or the subsequent separation procedures do not significantly affect the catalytic properties of the enzyme.

The quantification of MGL in the final conjugated product, P2, either by measuring the absorbance at 280 nm or by classical colorimetric protein quantification methods is very difficult due to AuNPs signal interference. Activity measurements led to estimate that 1.5–2 % of the initial enzymatic units of MGL are present in P2. Aware that some unbound MGL may still be present in P2, aliquots of this sample were centrifuged at higher speed (16,000 g for 10 min) to obtain complete precipitation of the MGL-AuNP complex and allow the recovery of a

colorless supernatant, S3 (Fig. SI3). Enzymatic activity measurements show that the amount of unbound MGL in S3 ranges from 10 % to 15 % of that contained in P2. Using the calibration curve shown in Fig. SI5 and assuming that the specific activity of the enzyme does not change upon interaction with AuNPs, the amount of active MGL tightly bound to AuNPs can be determined from the difference in activity between P2 and S3. We thus estimated the binding capacity of MGL, i.e., the number of MGL molecules bound per AuNP ($N_{MGL} = [MGL]_{bound}/[AuNPs]$), to be 5 $\pm$ 1. Geometrically, the maximum number of protein molecules (N_{Max}) that can adsorb as a monolayer on a single nanoparticle can be determined by:

$$N_{Max} = 4(R/r)^2 \quad (2)$$

where R and r are the radii of AuNP and MGL, respectively. For the AuNPs the estimated diameter is obtained by TEM and DLS measurements ($\Phi = 18$ nm), a value in good agreement with that obtained from SPR band spectral features. A diameter of 7.6 nm can be estimated for the MGL monomer, from the X-ray structure (PDB file 2RFV), while a diameter of 10 nm is calculated for the tetramer as the biological assembly generated by PISA software for the same PDB file. With these assumptions and according to Eq. (2), the maximum number of MGL bound per AuNP is 13, about 2.5 times higher than the value estimated by activity measurements. It should be emphasized that our estimated binding capacity refers only to the active protein, while partially active and/or denatured, therefore inactive, protein molecules may also occupy the surface of the AuNPs. The difference between the measured number of bound MGL molecules and the estimated upper limit might be thus in part ascribed to the formation of an inhomogeneous protein layer due to steric hindrance as well as to the presence of a fraction of partially active or inactive bound proteins, undetectable by activity measurements. We used circular dichroism to investigate the effect of conjugation on the structural integrity of MGL. The CD spectrum of MGL conjugated to AuNPs is compared to the CD spectrum of unconjugated MGL in solution in Fig. 3. Binding of MGL to AuNPs apparently induces a marked decrease in protein secondary structure content. In principle, this result could arise from a partial loss of structural integrity upon interaction with the AuNPs surface, or from a significant fraction of the AuNP-bound protein molecules having a strongly altered secondary structure, consistent with the discrepancy between the theoretical number of molecules covering AuNPs surface and the measured number of active molecules. However, the strong absorbance of AuNPs in the UV region prevents detailed quantitative analysis of data.

2.4. Physicochemical characterization of MGL-AuNP complex

Characterization of size and size distribution, state of dispersion, surface functionalization and influence of AuNPs on protein structure is of paramount importance since these properties determine the performance of nanomaterials, including the degree of protein adsorption, cellular uptake, biodistribution patterns, and clearance mechanisms (Nel et al., 2009).

Size and size distribution of AuNPs and MGL-AuNPs in solution were investigated through the AF4 system coupled to the DLS in flow mode. This instrumental setup is able to detect the presence of multiple populations in the samples and to measure the size of the separated particle fractions, thus improving the performance of the DLS measurement. Fig. 4 shows the combination of the UV–vis detector signal (at 525 nm) and the Z-average from the DLS measurement during the analysis of AuNPs and MGL-AuNPs. After conjugation, the particles show a longer retention time in the AF4 separation channel corresponding to a larger size (and/or changed surface properties) compared to protein-free AuNPs. In addition, MGL-AuNPs show a broad elugram only partially overlapping with the original AuNPs peak, which suggests that almost all AuNPs bind MGL. In specific, most of the MGL-AuNP population

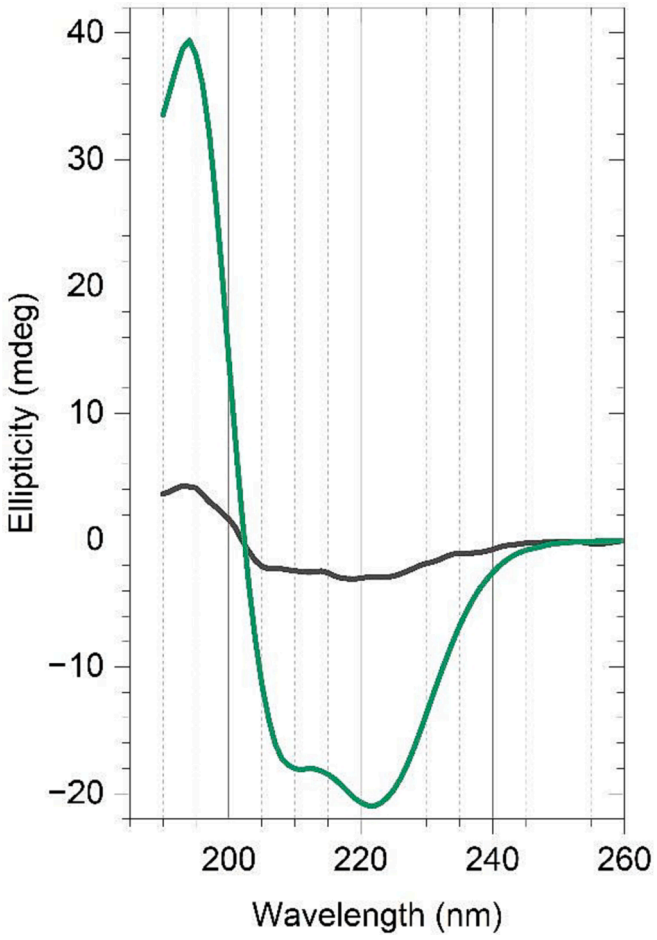

Fig. 3. CD spectra of MGL-AuNP complex (black line) compared to MGL in solution (dark green line). Spectra of 0.31 mM MGL-AuNPs and 25 μg/mL MGL were collected in water in a quartz cuvette with 0.5 cm path length. (For interpretation of the references to color in this figure legend, the reader is referred to the web version of this article.)

presents an elution time of 16 min and a hydrodynamic diameter of 35.3 $\pm$ 0.5 nm, while AuNPs elute at 13 min and have a hydrodynamic diameter of 24.5 $\pm$ 0.5 nm. These data, together with the TEM observations, suggest a hydration layer of about 3 nm in the presence of stabilizing citrate ions. Replacing the citrate with MGL results in the formation of a hydrated protein corona with about 7 nm thickness around the particles. This estimated thickness is lower than that expected for a closely packed protein monolayer (approximately 10 nm, diameter of the MGL in the tetrameric structure). This modest discrepancy between the expected and the measured layer thickness might be related to changes in the protein structure induced by the adsorption of MGL to the AuNP surface. Processes such as protein spreading and/or partial unfolding of a fraction of bound protein molecules can be hypothesized. These considerations on the structural changes of MGL following binding to AuNPs are supported by the CD data and the estimated number of active protein molecules below the maximum binding capacity.

The surface composition of the AuNPs and MGL-AuNPs is reported in Table 1. Table 1 also reports quantitative data related to MGL (398 amino acids, $C_{1900}H_{301}N_{519}O_{577}S_{16}$ MW 42877.9 g/mol) drop-casted on flat Au films. High resolution C1s, S2p, N1s core level spectra obtained by XPS analysis of MGL are shown in Fig. 5, whilst high-resolution core level spectra for AuNPs and MGL-AuNPs are compared in Fig. 6.

The analysis of the control MGL deposited on the Au film shows C, N, O concentrations in agreement with the theoretical values (Table 1). The

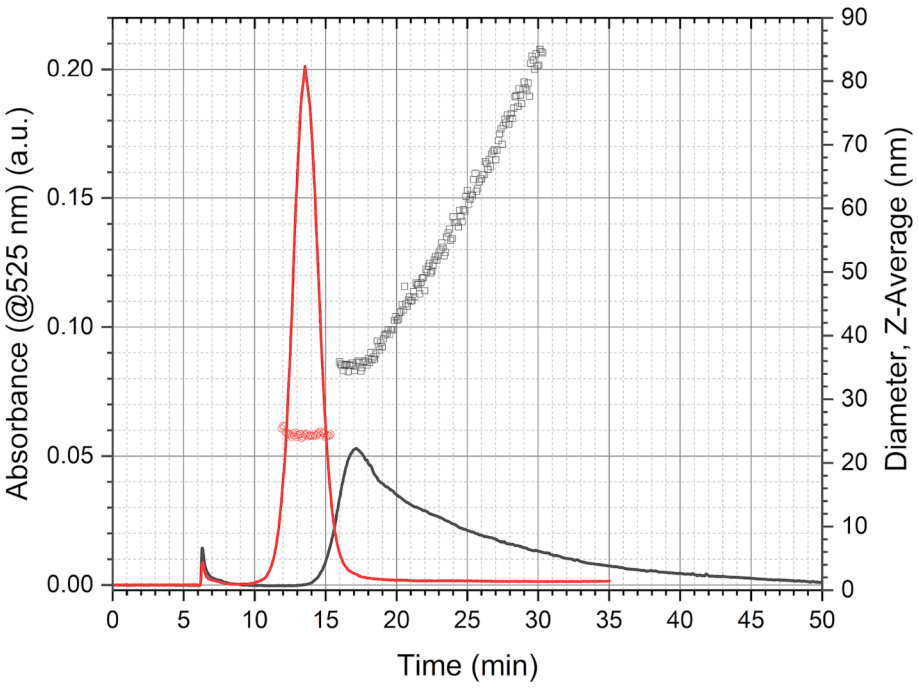

Fig. 4. AF4-DLS measurement of AuNPs (red) and MGL-AuNPs (black) showing UV–VIS detector absorbance signal (at 525 nm, continuous lines) on the left axis and the Z-average hydrodynamic diameters (dots) on the right axis. (For interpretation of the references to color in this figure legend, the reader is referred to the web version of this article.)

Table 1
Average and standard deviation values for samples elemental concentrations. Residual trace elemental signals to balance account collectively for about 1% of the total signal for each sample and are assigned to Si, K and Na. XPS survey spectra related to AuNPs and MGL-AuNPs are shown in Fig. SI6.

	Au (at.%)	O (at.%)	C (at.%)	N (at.%)	S (at.%)
AuNPs*	11.8 ± 2.6	13.4 ± 1.4	74.0 ± 2.6	–	–
MGL- AuNP	2.0 ± 0.1	23.0 ± 1.1	65.6 ± 1.9	9.3 ± 1.6	< 1**
MGL – Au_{film}	13.0 ± 1.6	14.7 ± 0.7	63.6 ± 0.7	8.7 ± 1.2	< 1**
MGL stoich.§	–	19.1	63.1	17.2	

* With citrate capping, measured after two centrifugation steps.
** Close to detection limit, not precisely quantifiable, < 1 %.
§ Stoichiometry calculated according to brute formula: $C_{1900}H_{301}N_{519}O_{577}S_{16}$.

slight difference in N, O and C theoretical and experimental concentrations can be ascribed to small amounts of surface hydrocarbon contamination at levels usually present in standard XPS samples preparation (Smith, 2005; Stevens et al., 2013; Walton et al., 2016). The quantitative analysis of AuNPs reveals a large amount of C and O attributable to the citrate capping. The analysis of the MGL-AuNP complex presents some interesting differences compared to the case of model MGL films deposited on Au flat surfaces: the nanoparticles show a strongly reduced Au signal, whilst the signals from the protein and the citrate layer (N1s, C1s and O1s) are increasing. In particular, N1s is specific to the bound protein and its ratio with the underlying Au substrate is increasing from $N/Au_{Film} = 0.6$ to $N/Au_{NP} = 4.8$. The increase could indicate that on AuNPs a denser protein layer is formed with respect to equivalent flat surfaces. Moreover, no sulfur signal was observed indicating that sulfur content of the attached MGL is below the detection limits of XPS. This is not surprising considering the low level of sulfur present in the protein (Table 1).

Analysis of the high-resolution core level spectra also provides information about the interaction between MGL and AuNPs. The C1s core level of MGL (Fig. 5a) can be fitted with 4 components, CC/CH (285 eV, 4, 1.5 %), C-O/C-N (286.3 eV, 36.9 %), C = O/C-O-N (288.2 eV, 15.3 %); COOH/COOR (289.2 eV, 1.7 %), respectively. A single doublet at about 163 eV ($S2p_{3/2}$), with a spin–orbit splitting of 1.3 eV, related to C-S bonding is observed on the S2p spectrum (Fig. 5b) (Das et al., 2012; Desimoni and Brunetti, 2015; Gordon et al., 2003). Finally, the N1s (Fig. 5c) shows two components at about 400 and 401 eV attributable to unprotonated and protonated amine/amide species, respectively (McArthur et al., 2014; Stevens et al., 2013; Vanea and Simon, 2011).

The C1s core level spectra of AuNPs show a completely different shape before and after interaction with MGL (Fig. 6a-b). In particular, the C1s spectrum of the bare AuNPs shows the presence of a major component at about 286.7 eV attributable to C-O citrate moieties and minor components related either to Au-COO^-, C = O and/or O-C-O bonds (287.8 eV, indicated globally as "COO" peak in Fig. 6) and COO (R) at 289.2 eV (La Spina et al., 2017; Park and Shumaker-Parry, 2015). However, a relatively strong component at 285.00 eV attributable to hydrocarbons is also observed. These data indicate that, beside the citrate molecules, other carbonaceous species likely introduced during the sample preparation are present on the nanoparticles surface. After the interaction of the MGL molecules with AuNPs, the C1s spectrum (Fig. 6b) changes dramatically showing an envelope typical of protein films and similar to that of the MGL sample reported in Fig. 5a (Belsey et al., 2015). These data support the quantitative analysis reported in Table 1 and indicate a quite strong interaction between the AuNPs and MGL with displacement of most of the citrate. In fact, the changes in the MGL secondary structure observed with the CD measurements also indicate a remarkable effect of the nanoparticles on the protein folding possibly related to the interaction of cysteines with AuNPs as well as to the relatively low pH used in this study.

The overlayer thickness of the citrate and MGL on the nanoparticles can be calculated from XPS data using a model proposed by A. Shard (Shard, 2012). This model calculates overlayer thicknesses using electron mean free path data, material electron densities and measured elemental concentration. For the core size of bare AuNPs, the diameter of 18.4 nm provided by TEM was used. Diameters estimated using TEM and XPS data for AuNPs and MGL-AuNPs are reported in Table 2. For reference, hydrodynamic diameters of AuNPs and MGL-AuNPs in

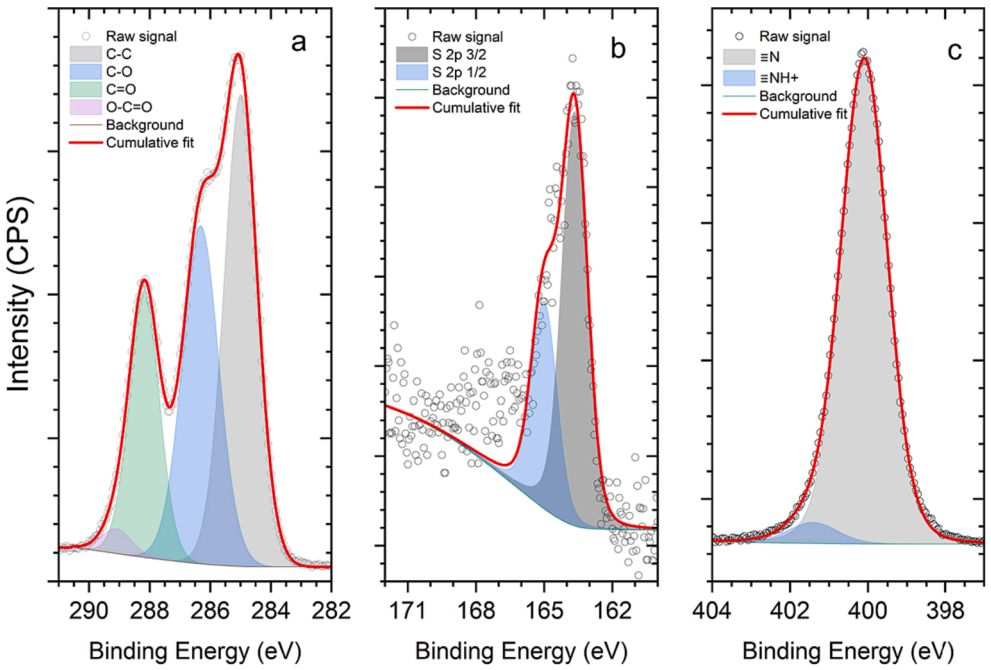

Fig. 5. High-resolution core level spectra of MGL protein film (a) C1s, (b) S2p and (c) N1s.

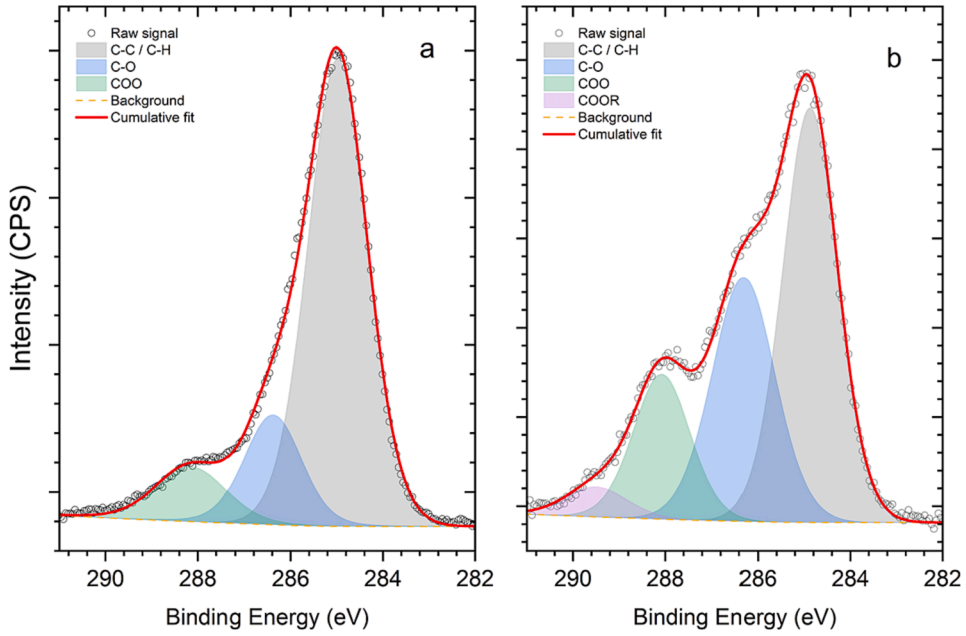

Fig. 6. C1s core level spectra of citrate stabilized AuNPs (a) and MGL-AuNPs (b).

solution measured by DLS coupled with AF4 are also reported in Table 2. In this Table the numerical results of the different sizing techniques are reported: AuNP metallic core size as measured indirectly by surface plasmon resonance wavelength (first column) and directly by TEM image analysis (second column); the protein shell thickness as measured by XPS using the electron attenuation lengths method (third column, total size NP is obtained adding the Au core diameter measured by TEM) and the total core–shell system hydrodynamic diameter as measured by AF4-DLS (fourth column). It is worth noting that a slight difference in the estimated diameter values is compatible with the different states of the sample: XPS experiments are performed in ultra-high vacuum ($p \sim 10^{-8}$ mbar) and water contribution is thus neglected, whilst AF4-DLS data refer to the hydrodynamic diameter. However, both techniques confirm at least one monolayer of protein molecules bound to the AuNPs. A coating thickness of about 3.15 nm was estimated by modeling XPS data measured onto dried samples. This value is similar to the data calculated from the difference (about 5.4 nm) between the hydrodynamic radii of nanoparticles with and without the MGL layer obtained in DLS-AF4 analysis.

2.5. *Protein stability in MGL-AuNP complex*

Maintenance of stability and biological activity of nanoparticle-conjugated proteins over time is a fundamental requirement to envision a therapeutic use. In order to evaluate how adsorption on AuNPs may affect MGL functionality, the enzyme activity over time of MGL-

Table 2
Comparison of the diameter of AuNPs, AuNP-citrate and MGL-AuNPs estimated using TEM, XPS, and DLS coupled with AF4.

	Diameters (nm)			
	SPR band	TEM	XPS[§]	AF4-DLS[*]
AuNPs [Φ_{core}]	18.0 ± 0.2	18.4 ± 1.2	–	–
AuNPs [$\Phi_{core\text{-}citrate}$]	–	–	22.4 ± 2.1	24.5 ± 0.5
MGL-AuNPs [$\Phi_{core\text{-}protein}$]	–	–	30.4 ± 6.5	35.3 ± 0.5
Protein Shell thickness [t_{shell}]	–	–	6.0 ± 0.9	8.6 ± 0.7

– not measured, not measurable.
[§] protein-shell thickness is measured with XPS, MGL-AuNPs diameter is calculated via $\Phi_{core\text{-}shell} = \Phi_{core} + 2{*}t_{shell}$. Samples are in a dry form.
[*] MGL-AuNPs hydrodynamic diameter is measured with AF4-DLS, protein-shell (hydrodynamic) thickness is calculated via $[\Phi_{core\text{-}shell} - \Phi_{core}]/2 = t_{shell}$.

AuNP complexes (P2) is compared to the activity of two different samples of MGL free in solution: $MGL_{untreated}$ (i.e., MGL never reacted with AuNPs), and S3 (the unbound MGL that remains in the supernatant upon the harsh centrifugation of P2). Fig. 7 shows the dependence of the residual activity, namely the activity normalized to that measured at time zero, over 7 days. It is evident that after one week for both samples of MGL free in solution ($MGL_{untreated}$ and S3), the activity is reduced by approximately 90 %, while the activity of the MGL-AuNP complex decreases slowly over time and maintains about half of its initial level over the same time range. These results indicate a relatively stable interaction between the catalytically active molecules of MGL and the AuNP surface, and preservation of the catalytic activity of the adsorbed protein over time, with respect to the free protein in solution maintained at the same conditions of temperature and pH.

To the best of our knowledge, there are few cases in the literature documenting the maintenance over time of the catalytic activity or the preservation of the structural properties of proteins adsorbed or conjugated to AuNPs (Capomaccio et al., 2016; Homaei and Etemadipour, 2015; Wang et al., 2020). Many benefits related to the immobilization of proteins on solid supports, including gold nanoparticles, have recently been reported (Chatterjee et al., 2021; Ellis et al., 2020; Verma et al., 2021). It has been proposed that multi-point attachment and/or restriction of protein mobility result in a thermodynamic or kinetic stabilization of the native state (Alam et al., 2021; Capomaccio et al., 2016; Chatterjee et al., 2021; Ellis et al., 2020; Ndlovu et al., 2020; Rodrigues et al., 2021; Verma et al., 2021; Weltz et al., 2020). Further, since the unfolded state occupies more space than the folded one, it has been hypothesized that the crowding effect induced by the high density of protein molecules on the nanoparticle surface can thermodynamically favor the folded state (Minton, 2001; Wang et al., 2020). Based on this hypothesis, the higher stability of the fraction of active MGL adsorbed on AuNPs might be attributed to conformational constraints to enzyme mobility, which delay the enzyme inactivation. Greater stability of MGL to chemical denaturation after encapsulation in silica gel was previously assessed and was related to the restriction of protein mobility within the confined space of the silica cage pores (Morozova et al., 2018).

3. Conclusions

The nano-conjugation of proteins to gold nanoparticles is an active area of research due to potential biomedical and nanotechnological applications. In this context, the most important feature to be assessed preliminarily to any other test in biological context is that the nano-conjugated proteins retain their native conformation as well as their functionality. Despite a wide body of investigations, current

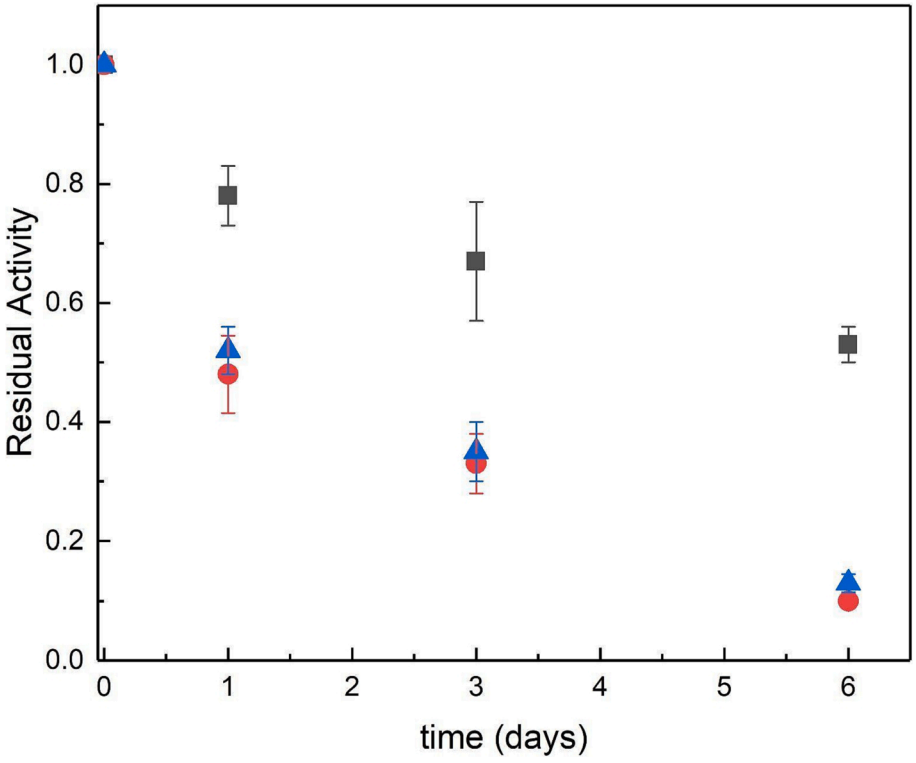

Fig. 7. Comparison over time of the residual catalytic activity of MGL bound to AuNPs (sample P2, black squares) and free in solution (sample S3, blue triangles; $MGL_{untreated}$, red circles) stored in 10 mM BTM/10 μM, pH 6, assayed in 100 mM KP, pH 8. S3 is the supernatant obtained from P2 centrifugation just before the activity measurements; $MGL_{untreated}$ is a sample of MGL stored in solution in the absence of AuNPs at the same temperature and pH conditions as P2. For each sample, the activity measured at different times was normalized to that measured at time zero. Error bars represent the standard deviation from three independent activity measurements. (For interpretation of the references to color in this figure legend, the reader is referred to the web version of this article.)

understanding of the protein–nanoparticles interactions is still limited, and a variety of behaviors have been observed. Indeed, whether proteins will retain their function upon adsorption appears to be a protein-specific effect difficult to predict. Hence, characterization of the protein-AuNP conjugates in terms of protein conformation, stability and function is of great interest.

In this paper, we report the first example of conjugation to 20-nm AuNPs of MGL, an enzyme capable of depleting methionine thus specifically reducing the survival of cancer cells. Different biophysical approaches were instrumental to prove the effective interaction of the protein with AuNPs and to characterize the particle size, particle distribution and surface properties of the conjugate. Indeed, data from TEM, AF4-DLS and XPS analysis are consistent with the presence of a protein monolayer stably adsorbed on the nanoparticle surface. A binding constant of 5×10^7 M^{-1} for the MGL-AuNP complex could be estimated by measuring the changes induced by MGL binding on the AuNP surface plasmonic resonance band. Circular dichroism measurements highlight the occurrence of changes in the protein secondary structure upon binding, at least for a fraction of the adsorbed protein molecules. Despite this, our data show that significant enzymatic activity of MGL was preserved upon formation of the MGL-AuNP complex and maintained over time longer than free protein in solution. We estimated at least 5 active MGL molecules adsorbed per nanoparticle, but partially inactive or denatured molecules are likely to contribute to the composition of the protein monolayer and the overall CD spectrum.

Indeed, preservation of catalytic activity and increased stability upon adsorption of enzymes to AuNPs are critical issues in the choice of the appropriate conjugation strategy and represent important advantages for the future prospective biomedical applications of our nanocomplex. Building on the encouraging results of this study, relevant questions regarding stability and activity in biological fluids will need to be addressed in the future to foster prospective therapeutic applications of MGL-AuNPs nanocomplexes.

4. Materials and methods

All chemicals were acquired from Sigma-Aldrich (Milan, Italy).

4.1. Expression and purification of methionine-γ-lyase (MGL)

E. coli BL21(DE3) cells containing the plasmid with the gene of *C. freundii* MGL were grown and the enzyme was purified according to the protocol previously described (Manukhov et al., 2006). Briefly, cells were suspended in the lysis buffer (100 mM KP pH 8.0 containing 0.1 mM PLP, 1 mM EDTA, and 5 mM DTT) and lysed by sonication. Cell debris was removed by centrifugation. A solution of 2 % (w/v) protamine sulfate was added to a final concentration of 0.33 % (w/v). The supernatant was applied to a HiPrep DEAE-Sepharose FF column equilibrated with the lysis buffer. The enzyme was eluted with the lysis buffer supplemented with 500 mM KCl, concentrated, and stored in lysis buffer at −80 °C. Before conjugation to AuNPs, aliquots of the MGL solution were transferred in 50 mM Bis-Tris Methane (BTM) plus 50 μM PLP, pH 6, by using centrifugal filter units 10,000 NMWL (Millipore, MA, USA). The concentration of MGL was determined by measuring the absorbance at 280 nm [$\varepsilon^{0.1\%} = 0.8$] (Morozova et al., 2010).

4.2. Enzymatic activity assay

The catalytic activity of MGL was measured by a discontinuous assay in 100 mM KP buffer, pH 8. Appropriate aliquots of protein were added to the substrate (L-Methionine, 25 mM final concentration) and incubated at 37 °C for 20 min. Then, 2,4-dinitrophenylhydrazine (DNPH) reagent (1 mM DNPH in 1 M HCl) was added to a final concentration of 0.3 mM, and incubated at 37 °C for 10 min. During this time, the α-ketobutyrate is derivatized as a phenylhydrazone. The color of the phenylhydrazone is developed by the addition of NaOH to a final concentration of 0.4 M. After mixing, the absorbance of the mixture was measured at 450 nm (Friedemann, 1943; Mesquita et al., 2014). The contribution at 450 nm due to any compounds, such as AuNPs or PLP, was duly subtracted.

4.3. Synthesis of gold nanoparticles (AuNPs)

Citrate-capped gold nanoparticles were synthesized following the procedure described (Frens, 1973; Turkevich et al., 1951), with some modifications. Briefly, aqueous solution of auric chloride ($HAuCl_4$, 1.2 M) and trisodium citrate dihydrate (Na_3-citrate, 0.038 M) were prepared. MilliQ deionized water (50 mL) was heated to the boiling point before the addition of 17 μL of $HAuCl_4$ solution. When the solution reached again the boiling point, Na_3-citrate (3.8 mL) was added. A light pink color appeared after a few minutes and gradually darkened to deep red purple. The resulting solution was allowed to boil for additional 20 min, under vigorous magnetic stirring. Then, AuNP suspension was slowly cooled to room temperature and afterwards purified by a centrifugation/resuspension process to decrease electrolyte and reaction side product concentration (Balasubramanian et al., 2010). Before starting the centrifugation process, 0.05 % Tween 20 was added to the suspension to avoid AuNP aggregation. Centrifugation period, speed and temperature were opportunely chosen to minimize nanoparticle aggregation and maximize the recovery. AuNP suspension was high-speed centrifuged (25000 rpm × 20 min, 20 °C) by an Optima™ L-90 K Ultracentrifuge (Beckam Coulter, USA), the supernatant was removed and replaced with an equal volume of MilliQ ultrapure water. The obtained suspension was again centrifuged at the same conditions. The second supernatant was almost completely removed obtaining about 2 mL of AuNP suspension with absorbance at 450 nm around 25. The adopted purification procedure allowed the recovery of almost all the synthesized AuNPs (95–98 %), as estimated by UV–vis absorbance measurements. Size and molar extinction coefficient at 450 nm of purified AuNPs were estimated from the UV–vis spectrum, according to Haiss et al., 2007 (Haiss et al., 2007). If the initially added Au^{3+} was completely reduced to Au^0, the gold concentration in the final suspensions was about 10 mM. Purified AuNP suspensions stored at 4 °C were stable over a long period (at least a year), as assessed by the unaltered UV–vis spectrum features.

4.4. UV–vis absorption measurements of MGL binding to AuNPs

Different concentrations of MGL ranging from 0 to 1.2 μM were incubated with 0.45 nM AuNPs in 10 mM BTM/10 μM PLP, pH 6. Addition of PLP, the coenzyme of MGL, is necessary to preserve the enzymatic activity. Samples were prepared directly in the plastic cuvettes subsequently used for absorption measurements, incubated at room temperature for 2 h and stored at 4 °C overnight. Binding of MGL to AuNPs was monitored by UV–vis absorption measurements in the range 350–800 nm at room temperature by a V-550 JASCO Spectrophotometer (JASCO, Japan).

4.5. Synthesis and purification of the MGL-AuNP complex

The synthesis reaction of MGL-AuNP complex was performed in low-binding microcentrifuge tubes. Aqueous AuNPs (100 μL, 4.57×10^{-8} M) were added to 500 μL of MGL (1.1 mg/mL) in 12 mM BTM/12 μM PLP, pH 6, to obtain a final 10 mM BTM/ 10 μM PLP buffer. The reaction mix was incubated at room temperature for 2 h and subsequently stored at 4 °C overnight. Then, MGL-AuNP suspension was centrifuged (10,000 *g* for 10 min) two times at 20 °C on an Eppendorf 5417R centrifuge (Eppendorf AG, Germany) to remove unbound MGL, following the scheme shown in Supporting Information (Fig. SI3). After the first centrifugation step, supernatant S1 was collected for further analysis while the pellet P1 was washed in 1.5 mL of 10 mM BTM/10 μM PLP buffer, pH 6, and centrifuged again under the same conditions.

Afterwards, the second supernatant (S2) was removed, and the pellet was conserved for the subsequent biochemical and spectroscopic characterization of the MGL-AuNP complex. MGL concentration in S1 and S2 was determined by measuring sample absorbance at 280 nm, corrected for AuNP contribution at this wavelength. S1, S2, P2 were also analyzed for MGL enzymatic activity.

4.6. Dynamic light scattering (DLS)

DLS measurements were carried out in a Zetasizer Nano ZS90 (Malvern, UK) to determine size and size distribution of synthetized AuNPs. Aliquots of 100 μL of AuNPs ([AuNPs] = 5×10^{-8} M) were diluted in 5 mL of MilliQ water and measurements were performed at 25 °C.

4.7. Scanning electron microscopy (SEM)

10 μL of 10^{-9} M AuNP suspension in MilliQ water were applied on a silicon oxide support and left overnight to dry in a N_2 atmosphere. SEM measurements were performed at 30 kV by SEM FE (Field Emission) JEOL 6500F (JEOL, Italy) and analyzed by the software ImageJ (NIH).

4.8. Transmission electron microscopy (TEM)

3 μL of AuNPs or MGL-AuNPs suspensions were deposited on Formvar Carbon coated 200 mesh copper grids (Agar Scientific, USA) and dehydrated overnight in desiccator before analysis at 120 kV by JEOL-JEM 2100 instrument (JEOL, Italy). Primary size distribution was assessed by counting at least 350 particles by ImageJ software coupled with Particle sizer plugin.

4.9. Asymmetrical flow field-flow fractionation (AF4) equipped with DLS (AF4-DLS)

Samples were concentrated by centrifugation to a nominal concentration of 1 mM. AF2000 Multiflow FFF system (Postnova Analytics) equipped with an on-line PN3212 spectrophotometer UV–vis detector (Postnova Analytics) and with an on-line DLS detector (Malvern) was used to measure the size distribution of AuNPs and MGL-AuNP complex. The AF4 channel had a 280 mm long separation channel, with 350 μm spacer. The membrane was made of regenerated cellulose with 10 kDa cut-off membrane. Particle suspensions were injected through a 100 μL loop in the AF4 channel using phosphate buffer 1 mM, pH 7.4 as carrier. The parameters for the AF4 separation were set as follow: during 5 min injection and focusing time, the sample flow was 0.25 mL min^{-1} with a focus flow of 1.25 mL min^{-1} and cross-flow of 1 mL min^{-1}. These conditions ensured the complete transfer of the sample. This step was followed by a 1-minute transition step to the starting conditions of the elution. The elution step started with a cross-flow of 1 mL min^{-1}, which decreased as a power function (exponent = 0.45) to 0.1 mL min^{-1} over 35 min and was kept constant for further 10 min. In each step, the outflow to the detector flow was set at 0.5 mL min^{-1}. The separation of MGL-AuNP particles to AuNPs were identified using the absorbance at 525 nm, which is specific for AuNPs localized surface plasmon resonance band.

4.10. Circular dichroism (CD)

Samples of MGL-AuNP complex and MGL in solution were diluted in Milli-Q H_2O to appropriate concentrations. MGL-AuNPs concentration was 0.31 mM and MGL was 25 μg/mL. Spectra were obtained at 25 °C with a Jasco-spectropolarimeter (Jasco CD J810, Inc., Easton MD, MA, USA) equipped with a Peltier temperature-controlled cell holder. Samples were loaded in a quartz cuvette with 0.5 cm optical length and each spectrum was obtained as an average of 4 scans, from 300 to 190 nm, with a 1-nm bandwidth pass and corrected for baseline contribution.

4.11. X-ray photoelectron spectroscopy (XPS)

For each sample, 150 μL of nanoparticle suspension was drop casted onto a clean Si substrate. The samples were dried in a desiccator and overnight in the load lock at p = 6.6×10^{-8} mbar before transfer in the analysis chamber. XPS measurements were performed in an Axis Ultra spectrometer (Kratos, Manchester, UK), using a Kα Al monochromatic source (hν = 1486.6 eV) operating at 150 W and X-ray spot-size of 400 × 700 μm^2 in hybrid mode. The residual pressure of the analysis chamber during the analysis was less than 1×10^{-8} mbar. For each sample, both survey spectra (0–1150 eV, pass energy 160 eV) and high-resolution spectra (pass energy at 20 eV) were recorded. Surface charge was compensated by a magnetic charge compensation system and the energy scale was calibrated by setting the C1s hydrocarbon peak to 285.00 eV. The take-off angle for the acquisitions was 90° with respect to the sample surface. The spectrometer was calibrated following the procedure described in the document (ISO, 2010).

The data were processed using Vision2 software (Kratos Analytical, UK) and the analysis of the XPS peaks was carried out using a commercial software package (Casa XPSv2023, Casa Software Ltd., UK). Peak fitting was performed with no preliminary smoothing. Asymmetric Gaussian–Lorentzian product functions were used to approximate the line shapes of the fitting components after a U 3 Tougaard-type background subtraction (Major et al., 2020).

CRediT authorship contribution statement

Samanta Raboni: Writing – review & editing, Writing – original draft, Methodology, Investigation, Funding acquisition, Conceptualization. **Francesco Fumagalli:** Writing – original draft, Investigation, Formal analysis. **Giacomo Ceccone:** Writing – review & editing, Resources, Formal analysis. **Rita La Spina:** Investigation, Formal analysis. **Jessica Ponti:** Investigation, Formal analysis. **Dora Mehn:** Methodology, Investigation, Formal analysis. **Giuditta Guerrini:** Investigation. **Stefano Bettati:** Writing – review & editing, Supervision, Resources. **Andrea Mozzarelli:** Writing – review & editing. **Mario D'Acunto:** Writing – review & editing. **Gianluca Presciuttini:** Investigation. **Caterina Cristallini:** Investigation. **Edi Gabellieri:** Writing – review & editing, Writing – original draft, Investigation, Formal analysis, Conceptualization. **Patrizia Cioni:** Writing – review & editing, Writing – original draft, Supervision, Resources, Conceptualization.

Declaration of competing interest

The authors declare that they have no known competing financial interests or personal relationships that could have appeared to influence the work reported in this paper.

Data availability

Data will be made available on request.

Acknowledgments

This research was granted to S.R. by University of Parma through the action Bando di Ateneo 2022 per la ricerca co-funded by MUR-Italian Ministry of Universities and Research – D.M. 737/2021 – PNR – PNRR – NextGenerationEU. Support was also provided by the Italian National Research Counil to P.C., E. G., M. D. and G. P.

The authors thank Prof G. Pennelli (Dipartimento di Ingegneria dell'Informazione, University of Pisa, Italy) for the scanning electron microscopy images, and Mr. A. Puntoni (IBF – CNR, Italy) for his technical contribution. Part of the experimental data used in this paper were generated through access to the Nanobiotechnology Laboratory under the Framework of access to the Joint Research Centre Physical Research Infrastructures of the European Commission.

Appendix A. Supplementary data

Supplementary data to this article can be found online at https://doi.org/10.1016/j.ijpharm.2024.123882.

References

Ajnai, G., Chiu, A., Kan, T., Cheng, C., Tsai, T., Chang, J., 2014. Trends of gold nanoparticle-based drug delivery system in cancer therapy. J. Exp. Clin. Med. 6, 172–178. https://doi.org/10.1016/j.jecm.2014.10.015.

Alam, S., Nagpal, T., Singhal, R., Kumar Khare, S., 2021. Immobilization of L-asparaginase on magnetic nanoparticles: kinetics and functional characterization and applications. Bioresour. Technol. 339, 125599 https://doi.org/10.1016/j.biortech.2021.125599.

Al-Johani, H., Abou-Hamad, E., Jedidi, A., Widdifield, C.M., Viger-Gravel, J., Sangaru, S. S., Gajan, D., Anjum, D.H., Ould-Chikh, S., Hedhili, M.N., Gurinov, A., Kelly, M.J., El Eter, M., Cavallo, L., Emsley, L., Basset, J.M., 2017. The structure and binding mode of citrate in the stabilization of gold nanoparticles. Nat. Chem. 9, 890–895. https://doi.org/10.1038/nchem.2752.

Amina, S.J., Guo, B., 2020. A review on the synthesis and functionalization of gold nanoparticles as a drug delivery vehicle. Int. J. Nanomed. 15, 9823–9857. https://doi.org/10.2147/ijn.s279094.

Anselmo, A.C., Mitragotri, S., 2016. Nanoparticles in the clinic. Bioeng. Transl. Med. 1, 10–29. https://doi.org/10.1002/btm2.10003.

Bailes, J., Gazi, S., Ivanova, R., Soloviev, M., 2012. Effect of gold nanoparticle conjugation on the activity and stability of functional proteins. Methods Mol. Biol. 906, 89–99. https://doi.org/10.1007/978-1-61779-953-2_7.

Balasubramanian, S.K., Yang, L.M., Yung, L.Y.L., Ong, C.N., Ong, W.Y., Yu, L.E., 2010. Characterization, purification, and stability of gold nanoparticles. Biomaterials 31, 9023–9030. https://doi.org/10.1016/j.biomaterials.2010.08.012.

Belsey, N.A., Shard, A.G., Minelli, C., 2015. Analysis of protein coatings on gold nanoparticles by XPS and liquid-based particle sizing techniques. Biointerphases 10. https://doi.org/10.1116/1.4913566.

Brancolini, G., Bellucci, L., Maschio, M.C., Di Felice, R., Corni, S., 2019. The interaction of peptides and proteins with nanostructures surfaces: a challenge for nanoscience. Curr. Opin. Colloid Interface Sci. 41, 86–94. https://doi.org/10.1016/j.cocis.2018.12.003.

Capomaccio, R., Osorio, I., Ojea-Jimenez, I., Ceccone, G., Colpo, P., Gilliland, D., Hussain, R., Siligardi, G., Rossi, F., Ricard-Blum, S., Calzolai, L., 2016. Gold nanoparticles increases UV and thermal stability of human serum albumin. Biointerphases 11. https://doi.org/10.1116/1.4972113.

Cavuoto, P., Fenech, M.F., 2012. A review of methionine dependency and the role of methionine restriction in cancer growth control and life-span extension. Cancer Treat. Rev. 38, 726–736. https://doi.org/10.1016/j.ctrv.2012.01.004.

Ceccone, G., Shard, A.G., 2016. Preface: in focus issue on nanoparticle interfaces. Biointerphases 11. Doi:10.1116/1.4972396.

Chatterjee, T., Das, G., Ghosh, S., Chakrabarti, P., 2021. Effect of gold nanoparticles on the structure and neuroprotective function of protein L-isoaspartyl methyltransferase (PIMT). Sci. Rep. 11 https://doi.org/10.1038/s41598-021-93752-1.

Chaturvedi, S., Hoffman, R.M., Bertino, J.R., 2018. Exploiting methionine restriction for cancer treatment. Biochem. Pharmacol. 154, 170–173. https://doi.org/10.1016/j.bcp.2018.05.003.

Cioni, P., Gabellieri, E., Campanini, B., Bettati, S., Raboni, S., 2022. Use of exogenous enzymes in human therapy: approved drugs and potential applications. Curr. Med. Chem. 29, 411–452. https://doi.org/10.2174/0929867328666210713094722.

D'Acunto, M., Cioni, P., Gabellieri, E., Presciuttini, G., 2021. Exploiting gold nanoparticles for diagnosis and cancer treatments. Nanotechnology 32, 192001. https://doi.org/10.1088/1361-6528/abe1ed.

Das, K.D., Dickinson, C., Lafir, F., Brougham, D.F., Marsili, E., 2012. Synthesis, characterization and catalytic activity of gold nanoparticles biosynthesized with Rhizopus oryzaeprotein extract. Green Chem 14, 1322–1334. https://doi.org/10.1039/C2GC16676C.

de la Fuente, M., Lombardero, L., Gomez-Gonzalez, A., Solari, C., Angulo-Barturen, I., Acera, A., Vecino, E., Astigarraga, E., Barreda-Gomez, G., 2021. Enzyme therapy: current challenges and future perspectives. Int. J. Mol. Sci. 22 https://doi.org/10.3390/ijms22179181.

Dean, S.N., Turner, K.B., Medintz, I.L., Walper, S.A., 2017. Targeting and delivery of therapeutic enzymes. Ther. Deliv. 8, 577–595. https://doi.org/10.4155/tde-2017-0020.

Derjaguin, B., 1941. Theory of the stability of strongly charged lyophobic sols and of the adhesion of strongly charged particles in solutions of electrolytes. Acta Physicochim. URSS 14, 633–662. https://doi.org/10.1016/0079-6816(93)90013-L.

Desimoni, E., Brunetti, B., 2015. X-ray photoelectron spectroscopic characterization of chemically modified electrodes used as chemical sensors and biosensors: a review. Chemosensors 3, 70–117. https://doi.org/10.3390/chemosensors3020070.

Dreaden, E.C., Mackey, M.A., Huang, X.H., Kang, B., El-Sayed, M.A., 2011. Beating cancer in multiple ways using nanogold. Chem. Soc. Rev. 40, 3391–3404. https://doi.org/10.1039/c0cs00180e.

Ellis, G.A., Dean, S.N., Walper, S.A., Medintz, I.L., 2020. Quantum dots and gold nanoparticles as scaffolds for enzymatic enhancement: recent advances and the influence of nanoparticle size. Catalysts 10. https://doi.org/10.3390/catal10010083.

El-Sayed, A.S., 2010. Microbial L-methioninase: production, molecular characterization, and therapeutic applications. Appl. Microbiol. Biotechnol. 86, 445–467. https://doi.org/10.1007/s00253-009-2303-2.

Fernandes, H.S., Teixeira, C.S.S., Fernandes, P.A., Ramos, M.J., Cerqueira, N., 2017. Amino acid deprivation using enzymes as a targeted therapy for cancer and viral infections. Expert Opin. Therap. Patents 27, 283–297. Doi:10.1080/13543776.2017.1254194.

Frens, G., 1973. Controlled nucleation for regulation of particle-size in monodisperse gold suspensions. Nat.-Phys. Sci. 241, 20–22. https://doi.org/10.1038/physci241020a0.

Friedemann, T.E., 1943. Pyruvic acid: II. The determination of keto acids in blood and urine. J. Biol. Chem. 147, 415–442.

Fung, M.K.L., Chan, G.C.F., 2017. Drug-induced amino acid deprivation as strategy for cancer therapy. J. Hematol. Oncol. 10 https://doi.org/10.1186/s13045-017-0509-9.

Gagner, J.E., Lopez, M.D., Dordick, J.S., Siegel, R.W., 2011. Effect of gold nanoparticle morphology on adsorbed protein structure and function. Biomaterials 32, 7241–7252. https://doi.org/10.1016/j.biomaterials.2011.05.091.

Gagner, J.E., Qian, X., Lopez, M.M., Dordick, J.S., Siegel, R.W., 2012. Effect of gold nanoparticle structure on the conformation and function of adsorbed proteins. Biomaterials 33, 8503–8516. https://doi.org/10.1016/j.biomaterials.2012.07.009.

Gasteiger E., H.C., Gattiker A., Duvaud S., Wilkins M.R., Appel R.D., Bairoch A., 2005. Protein Identification and Analysis Tools on the ExPASy Server. In: John M. Walker, (Ed.), The Proteomics Protocols Handbook, Humana Press, pp. 571–607.

Gay, F., Aguera, K., Senechal, K., Tainturier, A., Berlier, W., Maucort-Boulch, D., Honnorat, J., Horand, F., Godfrin, Y., Bourgeaux, V., 2017. Methionine tumor starvation by erythrocyte-encapsulated methionine gamma-lyase activity controlled with per os vitamin B6. Cancer Med. 6, 1437–1452. https://doi.org/10.1002/cam4.1086.

Ghosh, S.K., Pal, T., 2007. Interparticle coupling effect on the surface plasmon resonance of gold nanoparticles: from theory to applications. Chem. Rev. 107, 4797–4862. https://doi.org/10.1021/cr0680282.

Ghosh, P., Yang, X.C., Arvizo, R., Zhu, Z.J., Agasti, S.S., Mo, Z.H., Rotello, V.M., 2010. Intracellular delivery of a membrane-impermeable enzyme in active form using functionalized gold nanoparticles. J. Am. Chem. Soc. 132, 2642–2645. https://doi.org/10.1021/ja907887z.

Gordon, M.L., Cooper, G., Morin, C., Araki, T., Turci, C.C., Kaznatcheev, K., Hitchcock, A. P., 2003. Inner-shell excitation spectroscopy of the peptide bond: comparison of the C 1s, N 1s, and O 1s spectra of glycine, glycyl-glycine, and glycyl-glycyl-glycine. Chem. A Eur. J. 107, 6144–6159. https://doi.org/10.1021/jp0344390.

Guerrini, L., Alvarez-Puebla, R.A., Pazos-Perez, N., 2018. Surface modifications of nanoparticles for stability in biological fluids. Materials 11. https://doi.org/10.3390/ma11071154.

Haiss, W., Thanh, N.T.K., Aveyard, J., Fernig, D.G., 2007. Determination of size and concentration of gold nanoparticles from UV-Vis spectra. Anal. Chem. 79, 4215–4221. https://doi.org/10.1021/ac0702084.

Hodoroaba, V.D., Unger, W.E.S., Shard, A.G., 2020. Characterization of nanoparticles measurement processes for nanoparticles conclusions and perspectives. Doi: 10.1016/b978-0-12-814182-3.00006-7.

Hoffman, R.M., Erbe, R.W., 1976. High in vivo rates of methionine biosynthesis in transformed human and malignant rat cells auxotrophic for methionine. Proc. Natl. Acad. Sci. U.S.A. 73, 1523–1527. Doi:10.1073/pnas.73.5.1523.

Hoffman, R.M., 2015. Development of recombinant methioninase to target the general cancer-specific metabolic defect of methionine dependence: a 40-year odyssey. Expert Opin. Biol. Therapy 15, 21–31. Doi:10.1517/14712598.2015.963050.

Hoffman, R.M., 2019. Methionine Dependence of Cancer and Aging.Methods and Protocols Editors. Robert M. Hoffman.

Homaei, A., Etemadipour, R., 2015. Improving the activity and stability of actinidin by immobilization on gold nanorods. Int. J. Biol. Macromol. 72, 1176–1181. https://doi.org/10.1016/j.ijbiomac.2014.10.029.

Ielo, I., Rando, G., Giacobello, F., Sfameni, S., Castellano, A., Galletta, M., Drommi, D., Rosace, G., Plutino, M.R., 2021. Synthesis, chemical-physical characterization, and biomedical applications of functional gold nanoparticles: a review. Molecules 26. https://doi.org/10.3390/molecules26195823.

ISO 15472:2010, Surface chemical analysis—X-ray photoelectron spectrometers—Calibration of energy scales, 2010-05, Edition: 2. pp. 1–27.

Jazayeri, M.H., Amani, H., Pourfatollah, A.A., Avan, A., Ferns, G.A., Pazoki-Toroudi, H., 2016. Enhanced detection sensitivity of prostate-specific antigen via PSA-conjugated gold nanoparticles based on localized surface plasmon resonance: GNP-coated anti-PSA/LSPR as a novel approach for the identification of prostate anomalies. Cancer Gene Ther. 23, 365–369. https://doi.org/10.1038/cgt.2016.42.

Kopp, M., Kollenda, S., Epple, M., 2017. Nanoparticle-protein interactions: therapeutic approaches and supramolecular chemistry. Acc. Chem. Res. 50, 1383–1390. https://doi.org/10.1021/acs.accounts.7b00051.

Koval, V., Morozova, E., Revtovich, S., Lyfenko, A., Chobanian, A., Timofeeva, V., Solovieva, A., Anufrieva, N., Kulikova, V., Demidkina, T., 2022. Characteristics and stability assessment of therapeutic methionine gamma-lyase-loaded polyionic vesicles. ACS Omega 7, 959–967. https://doi.org/10.1021/acsomega.1c05558.

Kulikova, V.V., Morozova, E.A., Revtovich, S.V., Kotlov, M.I., Anufrieva, N.V., Bazhulina, N.P., Raboni, S., Faggiano, S., Gabellieri, E., Cioni, P., Belyi, Y.F., Mozzarelli, A., Demidkina, T.V., 2017. Gene cloning, characterization, and cytotoxic activity of methionine gamma-lyase from Clostridium novyi. IUBMB Life 69, 668–676. https://doi.org/10.1002/iub.1649.

Kumar, A., Dhawan, A., 2019. Nanoparticle-Protein Corona Biophysics to Biology Preface. Issues Toxicol 40, Vii-Vii Book. Doi:10.1039/9781788016308.

La Spina, R., Spampinato, V., Gilliland, D., Ojea-Jimenez, I., Ceccone, G., 2017. Influence of different cleaning processes on the surface chemistry of gold nanoparticles. Biointerphases 12. https://doi.org/10.1116/1.4994286.
Latour, R.A., 2015. The Langmuir isotherm: a commonly applied but misleading approach for the analysis of protein adsorption behavior. J. Biomed. Mater. Res. A 103, 949–958. https://doi.org/10.1002/jbm.a.35235.
Machover, D., Rossi, L., Hamelin, J., Desterke, C., Goldschmidt, E., Chadefaux-Vekemans, B., Bonnarme, P., Briozzo, P., Kopecny, D., Pierige, F., Magnani, M., Mollicone, R., Haghighi-Rad, F., Gaston-Mathe, Y., Dairou, J., Boucheix, C., Saffroy, R., 2019. Effects in cancer cells of the recombinant l-methionine gamma-lyase from brevibacterium aurantiacum. Encapsulation in human erythrocytes for sustained l-methionine elimination. J. Pharmacol. Exp. Ther. 369, 489–502. https://doi.org/10.1124/jpet.119.256537.
Major, G.H., Avval, T.G., Moeini, B., Pinto, G., Shah, D., Jain, V., Carver, V., Skinner, W., Gengenbach, T.R., Easton, C.D., Herrera-Gomez, A., Nunney, T.S., Baer, D.R., Linford, M.R., 2020. Assessment of the frequency and nature of erroneous x-ray photoelectron spectroscopy analyses in the scientific literature. J. Vac. Sci. Technol. A 38. https://doi.org/10.1116/6.0000685.
Manukhov, I.V., Mamaeva, D.V., Morozova, E.A., Rastorguev, S.M., Faleev, N.G., Demidkina, T.V., Zavilgelsky, G.B., 2006. L-methionine gamma-lyase from Citrobacter freundii: cloning of the gene and kinetic parameters of the enzyme. Biochemistry-Moscow 71, 361–369. https://doi.org/10.1134/s0006297906040031.
Marchetti, M., Faggiano, S., Mozzarelli, A., 2022. Enzyme replacement therapy for genetic disorders associated with enzyme deficiency. Curr. Med. Chem. 29, 489–525. https://doi.org/10.2174/0929867328666210526144654.
McArthur, S.L., Mishra, G., Easton, C.D., 2014. Applications of XPS in biology and biointerface analysis. In: Smentkowski, V.S. (Ed.), Surface Analysis and Techniques in Biology. Springer International Publishing, Cham, pp. 9–36. https://doi.org/10.1007/978-3-319-01360-2_2.
Mesquita, C.S., Oliveira, R., Bento, F., Geraldo, D., Rodrigues, J.V., Marcos, J.C., 2014. Simplified 2,4-dinitrophenylhydrazine spectrophotometric assay for quantification of carbonyls in oxidized proteins. Anal. Biochem. 458, 69–71. https://doi.org/10.1016/j.ab.2014.04.034.
Minton, A.P., 2001. The influence of macromolecular crowding and macromolecular confinement on biochemical reactions in physiological media. J. Biol. Chem. 276, 10577–10580. https://doi.org/10.1074/jbc.R100005200.
Mitchell, M.J., Billingsley, M.M., Haley, R.M., Wechsler, M.E., Peppas, N.A., Langer, R., 2021. Engineering precision nanoparticles for drug delivery. Nat. Rev. Drug Discov. 20, 101–124. https://doi.org/10.1038/s41573-020-0090-8.
Montalbano, S., Raboni, S., Sidoli, S., Mozzarelli, A., Bettati, S., Buschini, A., 2023. Post-translational modifications of histone variants in the absence and presence of a methionine-depleting enzyme in normal and cancer cells. Cancers 15. https://doi.org/10.3390/cancers15020527.
Moore, T.L., Rodriguez-Lorenzo, L., Hirsch, V., Balog, S., Urban, D., Jud, C., Rothen-Rutishauser, B., Lattuada, M., Petri-Fink, A., 2015. Nanoparticle colloidal stability in cell culture media and impact on cellular interactions. Chem. Soc. Rev. 44, 6287–6305. https://doi.org/10.1039/c4cs00487f.
Morozova, E.A., Bazhulina, N.P., Anufrieva, N.V., Mamaeva, D.V., Tkachev, Y.V., Streltsov, S.A., Timofeev, V.P., Faleev, N.G., Demidkina, T.V., 2010. Kinetic and spectral parameters of interaction of Citrobacter freundii methionine gamma-lyase with amino acids. Biochemistry-Moscow 75, 1272–1280. https://doi.org/10.1134/s0006297910100093.
Morozova, E.A., Kulikova, V.V., Yashin, D.V., Anufrieva, N.V., Anisimova, N.Y., Revtovich, S.V., Kotlov, M.I., Belyi, Y.F., Pokrovsky, V.S., Demidkina, T.V., 2013. Kinetic parameters and cytotoxic activity of recombinant methionine gamma-lyase from Clostridium tetani, Clostridium sporogenes, Porphyromonas gingivalis and Citrobacter freundii. Acta Nat. 5, 92–98.
Morozova, E.A., Kulikova, V.V., Faggiano, S., Raboni, S., Gabellieri, E., Cioni, P., Anufrieva, N.V., Revtovich, S.V., Demidkina, T., Mozzarelli, A., 2018. Soluble and nanoporous silica gel-entrapped C. freundii methionine gamma-lyase. J. Nanosci. Nanotechnol. 18, 2210–2219. https://doi.org/10.1166/jnn.2018.14333.
Mulvaney, P., 1996. Surface plasmon spectroscopy of nanosized metal particles. Langmuir 12, 788–800. https://doi.org/10.1021/la9502711.
Ndlovu, T., Ba, S., Malinga, S.P., 2020. Overview of recent advances in immobilisation techniques for phenol oxidases in solution. Catalysts 10. https://doi.org/10.3390/catal10050467.
Nel, A.E., Madler, L., Velegol, D., Xia, T., Hoek, E.M.V., Somasundaran, P., Klaessig, F., Castranova, V., Thompson, M., 2009. Understanding biophysicochemical interactions at the nano-bio interface. Nat. Mater. 8, 543–557. https://doi.org/10.1038/nmat2442.
Park, S.J., 2020. Protein-nanoparticle interaction: corona formation and conformational changes in proteins on nanoparticles. Int. J. Nanomed. 15, 5783–5802. https://doi.org/10.2147/ijn.s254808.
Park, J.W., Shumaker-Parry, J.S., 2014. Structural study of citrate layers on gold nanoparticles: role of intermolecular interactions in stabilizing nanoparticles. J. Am. Chem. Soc. 136, 1907–1921. https://doi.org/10.1021/ja4097384.
Park, J.W., Shumaker-Parry, J.S., 2015. Strong resistance of citrate anions on metal nanoparticles to desorption under thiol functionalization. ACS Nano 9, 1665–1682. https://doi.org/10.1021/nn506379m.
Raboni, S., Revtovich, S., Demitri, N., Giabbai, B., Storici, P., Cocconcelli, C., Faggiano, S., Rosini, E., Pollegioni, L., Galati, S., Buschini, A., Morozova, E., Kulikova, V., Nikulin, A., Gabellieri, E., Cioni, P., Demidkina, T., Mozzarelli, A., 2018. Engineering methionine gamma-lyase from Citrobacter freundii for anticancer activity. Biochimica et biophysica acta. Proteins Proteomics 1866, 1260–1270. https://doi.org/10.1016/j.bbapap.2018.09.011.
Raboni, S., Montalbano, S., Stransky, S., Garcia, B.A., Buschini, A., Bettati, S., Sidoli, S., Mozzarelli, A., 2021. A key silencing histone mark on chromatin is lost when colorectal adenocarcinoma cells are depleted of methionine by methionine gamma-lyase. Front. Mol. Biosci. 8 https://doi.org/10.3389/fmolb.2021.735303.
Rodrigues, R.C., Berenguer-Murcia, A., Carballares, D., Morellon-Sterling, R., Fernandez-Lafuente, R., 2021. Stabilization of enzymes via immobilization: Multipoint covalent attachment and other stabilization strategies. Biotechnol. Adv. 52, 107821 https://doi.org/10.1016/j.biotechadv.2021.107821.
Sengani, M., Grumezescu, A.M., Rajeswari, 2017. Recent trends and methodologies in gold nanoparticle synthesis – a prospective review on drug delivery aspect. OpenNano 2, 37–46.
Shard, A.G., 2012. A straightforward method for interpreting XPS data from core-shell nanoparticles. J. Phys. Chem. C 116, 16806–16813. https://doi.org/10.1021/jp305267d.
Shard, A.G., Wright, L., Minelli, C., 2018. Robust and accurate measurements of gold nanoparticle concentrations using UV-visible spectrophotometry. Biointerphases 13. https://doi.org/10.1116/1.5054780.
Shi, J.J., Kantoff, P.W., Wooster, R., Farokhzad, O.C., 2017. Cancer nanomedicine: progress, challenges and opportunities. Nat. Rev. Cancer 17, 20–37. https://doi.org/10.1038/nrc.2016.108.
Smith, G.C., 2005. Evaluation of a simple correction for the hydrocarbon contamination layer in quantitative surface analysis by XPS. J. Electron Spectrosc. Relat. Phenom. 148, 21–28. https://doi.org/10.1016/j.elspec.2005.02.004.
Raboni, S., Faggiano, S., Bettati, S., Mozzarelli, A., 2024. Methionine gamma-lyase: structure-activity relationship and therapeutic applications. Biochimica et Biophysica Acta (BBA) - Proteins and Proteomics Volume 1872, Issue 3, 1 140991 doi:org/10.1016/j.bbapap.2023.140991.
Souza, T.G.F., Ciminelli, V.S.T., Mohallem, N.D.S., 2015. A comparison of TEM and DLS methods to characterize size distribution of ceramic nanoparticles, 8th Brazilian Congress on Metrology (Metrologia), Bento Goncalvesalves, Brazil. Doi:10.1088/1742-6596/733/1/012039.
Stevens, J.S., de Luca, A.C., Pelendritis, M., Terenghi, G., Downes, S., Schroeder, S.L.M., 2013. Quantitative analysis of complex amino acids and RGD peptides by X-ray photoelectron spectroscopy (XPS). Surf. Interface Anal. 45, 1238–1246. https://doi.org/10.1002/sia.5261.
Tadepalli, S., Wang, Z., Slocik, J., Naik, R.R., Singamaneni, S., 2017. Effect of size and curvature on the enzyme activity of bionanoconjugates. Nanoscale 9, 15666–15672. https://doi.org/10.1039/c7nr02434g.
Tan, Y.Y., Xu, M.X., Hoffman, R.M., 2010. Broad selective efficacy of recombinant methioninase and polyethylene glycol-modified recombinant methioninase on cancer cells in vitro. Anticancer Res 30, 1041–1046.
Tong, R., Kohane, D.S., 2016. New Strategies in Cancer Nanomedicine, in: Insel, P.A. (Ed.), Annual Review of Pharmacology and Toxicology, vol. 56, pp. 41–57. doi: 10.1146/annurev-pharmtox-010715-103456.
Turkevich, J., Stevenson, P.C., Hillier, J., 1951. A study of the nucleation and growth processes in the synthesis of colloidal gold. Discuss. Faraday Soc. 11, 55–75. https://doi.org/10.1039/DF9511100055.
Vanea, E., Simon, V., 2011. XPS study of protein adsorption onto nanocrystalline aluminosilicate microparticles. Appl. Surf. Sci. 257, 2346–2352. https://doi.org/10.1016/j.apsusc.2010.09.101.
Vangala, K., Ameer, F., Salomon, G., Le, V., Lewis, E., Yu, L.Y., Liu, D., Zhang, D.M., 2012. Studying protein and gold nanoparticle interaction using organothiols as molecular probes. J. Phys. Chem. C 116, 3645–3652. https://doi.org/10.1021/jp2107318.
Verma, R., Singh, N., Chaudhuri, P., 2021. Stability and refolding of Dihydrofolate reductase enhances with nano-conjugation. Int. J. Biol. Macromol. 167, 987–994. https://doi.org/10.1016/j.ijbiomac.2020.11.053.
Verwey, E., 1948. Theory of the Stability of Lyophobic Colloids: The Interaction of Sol Particles Having an Electric Double Layer. Elsevier, Amsterdam. https://doi.org/10.1021/j150453a001.
Walton, J., Alexander, M.R., Fairley, N., Roach, P., Shard, A.G., 2016. Film thickness measurement and contamination layer correction for quantitative XPS. Surf. Interface Anal. 48, 164–172. https://doi.org/10.1002/sia.5934.
Wang, Y., Jonkute, R., Lindmark, H., Keighron, J.D., Cans, A.S., 2020. Molecular crowding and a minimal footprint at a gold nanoparticle support stabilize glucose oxidase and boost its activity. Langmuir 36, 37–46. https://doi.org/10.1021/acs.langmuir.9b02863.
Wang, A.L., Vangala, K., Vo, T., Zhang, D.M., Fitzkee, N.C., 2014. A three-step model for protein-gold nanoparticle adsorption. J. Phys. Chem. C 118, 8134–8142. https://doi.org/10.1021/jp411543y.
Wang, A.L., Perera, Y.R., Davidson, M.B., Fitzkee, N.C., 2016. Electrostatic interactions and protein competition reveal a dynamic surface in gold nanoparticle-protein adsorption. J. Phys. Chem. C 120, 24231–24239. https://doi.org/10.1021/acs.jpcc.6b08469.
Weltz, J.S., Kienle, D.F., Schwartz, D.K., Kaar, J.L., 2020. Reduced enzyme dynamics upon multipoint covalent immobilization leads to stability-activity trade-off. J. Am. Chem. Soc. 142, 3463–3471. https://doi.org/10.1021/jacs.9b11707.
Wilson, B.K., Prud'homme, R.K., 2021. Nanoparticle size distribution quantification from transmission electron microscopy (TEM) of ruthenium tetroxide stained polymeric nanoparticles. J. Colloid Interface Sci. 604, 208–220. https://doi.org/10.1016/j.jcis.2021.04.081.
Xia, Z.H., Villarreal, E., Wang, H., Lau, B.L.T., 2020. Nanoscale surface curvature modulates nanoparticle-protein interactions. Colloids Surf. B-Biointerfaces 190. https://doi.org/10.1016/j.colsurfb.2020.110960.
Xin, L., Yuan, Y.W., Liu, C., Zhou, L.Q., Liu, L., Zhou, Q., Li, S.H., 2021. Preparation of internalizing RGD-modified recombinant methioninase exosome active targeting

vector and antitumor effect evaluation. Dig. Dis. Sci. 66, 1045–1053. https://doi.org/10.1007/s10620-020-06262-x.

Yang, J.A., Johnson, B.J., Wu, S., Woods, W.S., George, J.M., Murphy, C.J., 2013. Study of wild-type alpha-synuclein binding and orientation on gold nanoparticles. Langmuir 29, 4603–4615. https://doi.org/10.1021/la400266u.

Yeh, Y.C., Creran, B., Rotello, V.M., 2012. Gold nanoparticles: preparation, properties, and applications in bionanotechnology. Nanoscale 4, 1871–1880. https://doi.org/10.1039/c1nr11188d.